

Migration of DNA molecules through entropic trap arrays: a dissipative particle dynamics study

E. Moeendarbary · T. Y. Ng · H. Pan ·
K. Y. Lam

Received: 5 March 2009 / Accepted: 24 May 2009 / Published online: 19 June 2009
© Springer-Verlag 2009

Abstract Dissipative particle dynamics (DPD) simulations of worm-like chain bead-spring models are used to explore the electrophoresis migration of DNA molecules traveling through narrow constrictions. The DPD is a relatively new numerical approach that is able to fully incorporate hydrodynamic interactions. Two mechanisms are identified that cause the size-dependent trapping of DNA chains and thus mobility differences. First, small molecules are found to be trapped in the deep region due to higher Brownian mobility and crossing of electric field lines. Second longer chains have higher probability to form hernias at the entrance of the gap and can pass the entropic barrier more easily. Consequently, longer DNA molecules have higher mobility and travel faster than shorter chains. The present DPD simulations show good agreement with existing experimental data as well as published numerical data.

Keywords Dissipative particle dynamics · Entropic trap · DNA molecules · Worm-like Chain · Brownian motion · Hernia nucleation

1 Introduction

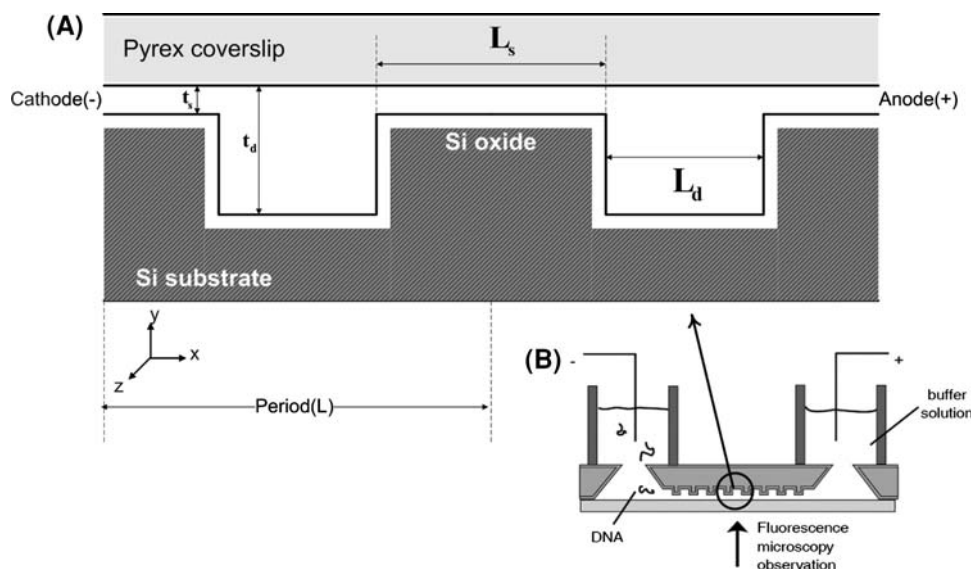
Microfluidics and more recently Nanofluidics are advancing fields traversing over vast areas of engineering, physics, chemistry and biotechnology. More importantly, micro/nano devices are fabricated in order to carry out highly

efficient as well as simultaneous analysis of particles, molecules or cells such as in genomic, proteomic, and metabolic applications in biotechnology. In particular, the DNA separation process is important for various biological analyses, such as DNA fingerprinting and genome sequencing. Advances in the field of micro-total analysis systems (μ -TAS) and especially lab-on-a-chip devices provide many researchers with the capability to propose novel separation mechanisms using these micro- and/or nano-fluidic devices. For efficient separation without the use of gel matrices or pulsed electric fields, Han et al. (1999), Han and Craighead (2000, 2002), designed and fabricated an entropic trapping array, consisting of alternative deep and shallow channels, to separate long DNA molecules (>2 kbp). These silicon based periodic constriction channels are fabricated using standard etching techniques and are enclosed with a Pyrex cover plate as shown in Fig. 1. The DNA molecules are suspended in the cathode side of the device which is filled with buffer solution before the start of the separation process. The DNA molecules start traveling from the cathode towards the anode when a dc electric field is applied. The shallow section is much smaller than the moving molecules' radius of gyration such that the molecules must change their conformations and uncoil in order to pass through the channel. This process creates electrophoretic mobility differences, thus enabling efficient separation.

Achieving appropriate and optimized design for specific application requires advancements of the related electro-mechanical devices, in terms accuracy and speed of analysis. The development of micro- and nano-electromechanical systems (MEMS/NEMS) is leading to the need for continuous improvements in modeling approaches so as to obtain a better understanding of the underlying physical and chemical effects. Numerical simulation is a way to

E. Moeendarbary · T. Y. Ng (✉) · H. Pan · K. Y. Lam
School of Mechanical and Aerospace Engineering,
Nanyang Technological University, 50 Nanyang Avenue,
Singapore 639798, Singapore
e-mail: mtyng@ntu.edu.sg

Fig. 1 Schematic diagram of the nanofluidic separation device [adapted from (Han et al. 1999; Han and Craighead 2000, 2002)]. **a** Cross-section of two period of the device, **b** experimental setup



model these complex systems, which usually involve the simulation of coupled energy domains, such as mechanical (structural), fluidic, thermal, electrical, optical and magnetic fields. Simulation of complex fluidic systems, especially those with suspension of different particles/macromolecules, is not easy due to the involved complex features, including movable boundaries, large surface-to-volume ratio, and physical microscale phenomena. Mesoscopic fluid simulations bridge the gap between atomistic simulations and macroscopic network simulations (Groot and Warren 1997), and overcome the inherent difficulties faced by conventional methods when applied to complex fluids. The aim of these intermediary simulation techniques is to identify characteristic physical lengths and times in the system in order to use them for complex model simplification. The dissipative particle dynamics (DPD) is a potentially very powerful and simple mesoscopic approach, which facilitates the simulation of the statics and dynamics of complex fluid and soft matter systems at physically interesting length and time scales.

In this paper, we applied the DPD method to reproduce the translocation of DNA strands through the geometry as shown in Fig. 1. We should emphasise that our aim is to understand the underlying nature of the separation process using the new technique (the DPD), and in this paper we are not concerned about fitting any specific experimental data or quantitative discrepancies. To ensure that the process is in the proper regime, the simulations were attempted to be at some level that we can establish a reliable qualitative correspondence with experiments. We employed DPD due not only to its relatively larger time- and length-scales (compared to molecular simulation techniques), but also its ability to inherently capture the rheological properties of complex fluid and soft matter systems quite straightforward compared to other conventional methods. Furthermore,

DPD model allows inclusion of the solvent molecules explicitly so that the electroosmotic flow (EOF) effects and the hydrodynamic interactions can be handled with ease. In the current work, we focused only on the latter aspect which is inherently captured through standard DPD algorithm, while being aware that the potential inclusion of EOF in the DPD model is an interesting future perspective for further work.

2 Entropic trapping: theoretical and numerical background

In the trapping array device of Han et al. (1999), Han and Craighead (2000, 2002), the authors observed counterintuitive phenomenon in that “longer DNA molecules found to escape faster than shorter one”. They proposed a simple kinetic theory [hernia nucleation in (Tessier et al. 2002) or beachhead scenario in (Cheng et al. 2008)] to obtain more insight into the separation mechanism. Crossing over the thin region of the channel requires the overcoming of the entropic barrier. The existence of this barrier is due to the conformational change and uncoiling of the DNA in the gap which reduces the entropic elasticity of the chain. The electric field drives the DNA towards the gap and the high intensity field region of the gap sucks the chain hernias at the entrance of the gap. The longer chains have higher probability of the monomers contacting the gap region and thus the rate of escape for long DNA strands is higher than shorter ones. In (Han and Craighead 2002), the following simple expression for the trapping time of the chain was proposed:

$$\tau_{\text{trap}} = \tau_0 \exp(\alpha/E_s k_B T) \quad (1)$$

where E_s is the electric field strength in shallow region, T the temperature, k_B the Boltzmann constant and α a

constant that depends solely on the experimental setup conditions and is not a function of the length of the chains. The τ_0 is dependent on the strength of electric field and chain length in such a way that τ_0 decreases as the DNA size increases and this implies the size-selective separation of the designed microfluidic device. Based on Eq. 1, the authors of Han and Craighead (2002) predicted that the trapping time and more specifically the selectivity depends on structural parameters such as the depths of the wells and shallow regions, the length of channels, as well as the strength of applied electric field, and they also proved this experimentally.

Besides some of the mentioned experimental studies, numerical simulation provides an alternative route to study DNA separation processes which involve different time- and length-scales. The micro-channels used in the DNA separation have characteristic size from dozens of nanometers to several micrometers. In addition, traveling and conformation change of DNA in each trap is in the micro-second time scale regime, while the total experimental time is of the order of several minutes. Due to the molecular scales involved, direct simulation techniques, such as molecular dynamics (MD) on large scales, are very expensive if not totally unfeasible. Furthermore, the mechanical properties of DNA are actually physically relevant at mesoscopic scale (0.1 μm) level and can thus be used for understanding the separation process. Apart from DPD, the Monte Carlo (MC) method and the more widely used Brownian Dynamics (BD) simulation are examples of mesoscopic numerical techniques that have been applied in this area.

Using the Monte Carlo technique, Tessier et al. (2002) simulated the flow of DNA through entropic trap arrays where the polymer is modeled by a lattice model with bond fluctuation. Their results mostly confirmed the qualitative observation of Han et al. (1999), Han and Craighead (2000, 2002) that longer molecules were trapped for a shorter time due to high probability of hernia nucleation and the deformation of molecules at the gap entrance. In the Monte Carlo simulation of Chen and Escobedo (2003), the free-energy barrier for escape ΔF_{max} as a function of chain length was examined in different electric field regimes, and in the intermediated fields ($\Delta F_{\text{max}} \sim k_{\text{B}}T$) they confirmed that trapping lifetime decreases as the chain length increases. In addition, they showed that in weak electric fields the main controlling factor in the escape process is the $\exp(\Delta F_{\text{max}}/k_{\text{B}}T) = \exp(\alpha/E_s k_{\text{B}}T)$ term while at moderate to strong fields τ_0 is the dominant prefactor.

Streek et al. (2004) performed BD simulations and found two key mechanisms which contribute to longer trapping lifetimes for smaller molecules, namely the probabilistic delayed entry of the short chains at the entrance of constriction and the diffusion of small

molecules to the corner of the well. Panwar and Kumar (2006) have arguably carried out the most comprehensive work in characterizing time scales involving electrophoresis of polymer chains through constrictions. They found that the approach time τ_{app} , which is related to the motion of the polymer in the deep region towards the entrance of constriction, and activation time τ_{act} , which defines the time scale for overcoming entropic barrier, are both decreased as the sizes of the molecules become larger. However, the traveling time through the shallow region τ_{cross} , increased upon increase of the length of the chains. More recently and in similar manner, Lee and Joo (2007) used the worm-like chain (WLC) models and performed BD numerical experiments for the electrophoretic motions of both linear and branched polyelectrolyte molecules traversing entropic traps. In addition, they applied the coarse-grained bead spring model to investigate the effects of polymer topology and found the radius of gyration to be the dominant factor influencing time scales during the escape of polymers.

In most of the above simulations, several important physical phenomena (such as hydrodynamic interactions, EOF contributions, electrostatic interactions and excluded volume effects) were not considered. Neglecting some of these phenomena can be quite reasonable when the separation mechanisms are investigated more qualitatively. However, some of the other parameters, as we shall discuss in the following, play such an important role that can affect the overall results and are thus not negligible.

According to Streek et al. (2005), the surface of the channel walls may be negatively charged during the experiment generating the electroosmotic flow and this slows down the DNA molecules migrating towards the anode. In addition to EOF effects at the walls, there exists a local EOF generated by the counter-ions surrounding the DNA chain (Viovy 2000; Long et al. 1996). This effect was neglected in the mentioned simulations by the claim that in the experimental conditions the induced forces from the electroosmotic flow on chains segments were found to be weak. However, electroosmotic flow is strengthened in intense electric fields and high-buffer concentrations which lead to converging or diverging flow patterns as well as circulation. Although we have not considered EOF in the current simulations, the DPD algorithm is capable of capturing it with ease.

In most of the previous studies, the DNA and solvent hydrodynamic interactions were neglected. Also both hydrodynamic and electrostatic interactions between the chains and the walls were disregarded. The assumption was made following the argument that the induced friction by the motion of the counter ions cancels the hydrodynamic flow generated by the migration of chain segments in the cases of free solution electrophoresis. However, according

to Viovy (2000), hydrodynamic interaction is not negligible for DNA undergoing electrophoresis. Jendrejack et al. (2002) also claimed that a hydrodynamic interaction model will generate results which are in qualitative agreement with experimental data. Walls always induce hydrodynamic effects, thus affecting flow patterns as well as chain trajectories, so the cancelation argument is not valid if the chain is blocked by an obstacle (Long et al. 1996; André et al. 1998), and this is the case especially near the entrance of the constriction. Moreover, the walls are being charged during the process and have some electrostatic effects, especially during the migration of the polymer through the shallow region (with thickness of usually less than 100 nm) and when the chain contacts or are very close to the wall boundaries.

Debye screening length of DNA in usual buffer solutions is of the order of a few nanometers. However, the persistence length of DNA is about 50 nm, thus electrostatic interactions between monomers can generally be omitted. Some authors have not taken into account the excluded volume interactions. However, it is obvious that the chain segments do not overlap each other and cannot occupy the same space/position.

Bearing in mind the above restrictions, we investigate an alternative approach in order to simulate the migration of DNA through constriction. We find that the dissipative particle dynamics (DPD) method, which is a mesoscopic method that can bridge the gap between atomistic simulations and continuum level simulations, to be an ideal tool to explore this migration process. Using the DPD technique with appropriate parameters, we naturally captured some of the dynamical and rheological properties, such as the hydrodynamic interactions, the DNA-wall interactions and excluded volume effects (Jiang et al. 2007; Pan et al. 2008; Li and Drazer 2008; Fedosov et al. 2008). It should be noted that in the above BD and MC numerical simulations, even by neglecting some of the underlying natural phenomena, the authors were able to show some agreeable qualitative results with experimental data. However, the DPD technique inherently incorporates physical aspects and enables us to obtain more matchable results, both qualitatively and quantitatively. In particular, the DPD is becoming noted as a promising and powerful method for the simulation of complex fluids such as suspensions of DNA and polymers, and it is also easier to simulate some other complex phenomena such as EOF effects with DPD than other techniques. In this work, we are looking at the process as a whole with the aim of identifying the important mechanisms of DNA translocation with the DPD model. Detailed characterization of the process such as full investigation of the characteristic times (τ_{app} , τ_{act} and τ_{cross}), center of mass density distributions of the chain, the DNA depletion and migration through thin channels,

effects of solvent quality and Schmidt number, explicit inclusion of EOF, etc., can be a numerically very demanding, and they represent possible future work in this area, requiring extra numerical effort as well as more detailed experimental data for comparison, and is, therefore, out of scope of the current work.

3 Description of the present simulation model and parameters

3.1 Dissipative particle dynamics algorithm

The dissipative particle dynamics (DPD) technique is an alternative method for mesoscopic fluid simulation, which was first introduced by Hoogerbrugge and Koelman (1992), and was later modified by Espanol and Warren (1995). Since 1990, when the DPD method was first developed in Europe, the DPD has been applied in the study of the dynamical properties of a wide variety of systems and applications such as rheological properties of polymers/macromolecules, morphologies and mesophase separation of block copolymers, formation of lipid bilayer and biological membranes, self-assembling systems of surfactants and amphiphiles, colloidal systems and immiscible fluids, multiphase flows, etc. Recently, a lot of attention has been given to macromolecular transport in micro/nano channels due to wide variety of applications in chromatography and electrophoresis separation devices. The existence of complex geometries and coupling of fluid flow with other external force fields in these devices make DPD one of the best alternative simulation techniques to study the dynamical behaviors of these systems. Using a DPD model of finitely extendable nonlinear elastic (FENE) chain, Fan et al. (2003) were able to fit the velocity profiles of FENE chain suspensions with power-law curves. Later in Fan et al. (2006), DNA suspension flow through a microchannel was modeled employing DPD simulations of worm-like chains. The DPD results of worm-like chains under shear flow matched well with the single DNA experiments (Symeonidis et al. 2005). Millan et al. (2007) studied the effects of bead number, polymer concentration, and flow rate on the streaming of polymer solution in pressure driven flow. Employing two-dimensional DPD simulations, the effects of field strength, chain length, solvent quality, and pore size were explored for the translocation of a single polymer chain through a pore under a fluid field (He et al. 2007).

The DPD algorithm is a combination of molecular dynamics, Brownian dynamics and lattice gas automata, and derives its static and dynamic properties according to the theory of statistical mechanics (Marsh et al. 1997). Similar to molecular dynamics, the time evolution of each

DPD particle, which represents a cluster of molecules/atoms, can be calculated by Newton’s second law

$$\frac{d\mathbf{r}_i}{dt} = \mathbf{v}_i, \quad \frac{d\mathbf{p}_i}{dt} = \sum_{j \neq i} \mathbf{F}_{ij}, \quad (2)$$

where \mathbf{r}_i , \mathbf{v}_i and $\mathbf{p}_i = m\mathbf{v}_i$ are, respectively, the position, velocity, and momentum vectors of particle i , and \mathbf{F}_{ij} is the total interparticle force exerted on particle i by particle j . In this work we normalize the mass of each particle m_i , to be unity. The interparticle force, $\mathbf{F}_{ij} = \mathbf{F}_{ij}^C + \mathbf{F}_{ij}^D + \mathbf{F}_{ij}^R$ is defined by three components that lie along their lines of centers and conserves linear and angular momentum: a purely repulsive conservative force $\mathbf{F}_{ij}^C = w^C(r_{ij}) \mathbf{e}_{ij}$, a dissipative or frictional force $\mathbf{F}_{ij}^D = -\gamma w^D(r_{ij}) [\mathbf{v}_{ij} \cdot \mathbf{e}_{ij}] \mathbf{e}_{ij}$ which slows down the particles motion with respect to each other and represents the effects of viscosity, and the random or stochastic force $\mathbf{F}_{ij}^R = \sigma w^R(r_{ij}) \theta_{ij} \mathbf{e}_{ij}$ which provides the thermal or vibrational energy of the system, where $\mathbf{e}_{ij} = \mathbf{r}_{ij}/r_{ij}$, $\mathbf{r}_{ij} = \mathbf{r}_i - \mathbf{r}_j$, $r_{ij} = |\mathbf{r}_i - \mathbf{r}_j|$ and $\mathbf{v}_{ij} = (\mathbf{v}_i - \mathbf{v}_j)$. w^C , w^D and w^R are the conservative, dissipative, and random r dependent weight functions. The θ_{ij} term is a Gaussian white noise function with symmetry property $\theta_{ij} = \theta_{ji}$ to ensure the total conservation of momentum and has the following stochastic properties, namely: $\langle \theta_{ij}(t) \rangle = 0$ and $\langle \theta_{ij}(t) \theta_{kl}(t') \rangle = (\delta_{ik} \delta_{jl} + \delta_{il} \delta_{jk}) \delta(t - t')$.

All of the above forces are acting within a sphere of interaction or cutoff radius r_c which is the length scale parameter of the system. The γ and σ are the coefficients of the dissipative and random forces, respectively. Similar to the fluctuation–dissipation theorem (Kubo 1966), Espanol and Warren (1995) obtained the detailed balanced condition for the DPD as

$$w^D(r) = [w^R(r)]^2, \quad \sigma^2 = 2\gamma k_B T/m, \quad (3)$$

where k_B is the Boltzmann constant and T the equilibrium temperature. The conservative force weight function is given by $w^C(r_{ij}) = a_{ij} (1 - r_{ij}/r_c)$ when $r_{ij} \leq r_c$ and zero otherwise, where $a_{ij} = \sqrt{a_i a_j}$ is the repulsion parameter. We can match the compressibility condition and determine the repulsion parameter as a function of DPD number density ρ and system temperature which is applicable for fluid–fluid interactions (Groot and Warren 1997; Groot and Rabone 2001)

$$a_f = a_{ff} = 75k_B T/\rho_f \quad (4)$$

The dissipative and random weight functions take the general form Fan et al. (2006)

$$w^D(r_{ij}) = [w^R(r_{ij})]^2 = \begin{cases} \left(1 - \frac{r_{ij}}{r_c}\right)^s & r_{ij} \leq r_c \\ 0 & r_{ij} \geq r_c \end{cases} \quad (5)$$

In the present DPD simulation, we set the exponent parameter to $s = 2$. The random force transforms to $F_{ij}^R =$

$\sigma w^R(r_{ij}) \zeta_{ij}/\sqrt{dt} \mathbf{e}_{ij}$, where ζ_{ij} represents an independent increment in a stochastic process, which is represented by a uniform distribution of random numbers whose mean is zero with unit variance, and generated independently for different pairs of particles at each time step. In the present DPD simulations, we used the non-dimensional standard DPD parameters (Groot and Warren 1997; Espanol and Warren 1995) as $k_B T = 0.2$, $\rho_f = 4$, $r_c = 1$ and $\sigma = 3$. The dimensional parameters and scale up factors can be adjusted by comparing the static and dynamic properties of the simulated solvent or polymer (such as shear viscosity, diffusion coefficients, polymer length and relaxation time) with that of the real system. We chose the length unit to be $[r_c] = 50$ nm so that the chains with maximum segment length of 2 and bead numbers of 5–320 to represent DNAs of length 1.18–93.8 kbp, respectively. Setting up the mass and energy units as $[m] = 5 \times 10^{-15}$ and $[k_B T] = 4.14 \times 10^{-21}$ J for $T = 300$ K, time unit $[t]$ can be calculated directly $\sqrt{m r_c^2/k_B T} \approx 5.5 \times 10^{-5}$ s. Hence 1 s corresponds to $\sim 10^6$ time steps with the chosen time increment of $dt = 0.02$. These units allow us to model systems with length scales from nanometers to micrometers and overall time scales of up to a few seconds. The time evolution of the system (including both chain and solvent particles) is computed using the velocity-Verlet algorithm with the suggested $\lambda = 0.65$ (Groot and Warren 1997)

$$\begin{aligned} \mathbf{r}_i^{t+dt} &= \mathbf{r}_i^t + dt \mathbf{v}_i^t + \frac{1}{2} dt^2 \mathbf{f}_i^t \\ \tilde{\mathbf{v}}_i^{t+dt} &= \mathbf{v}_i^t + \lambda dt \mathbf{f}_i^t \\ \mathbf{f}_i^{t+dt} &= \mathbf{f}_i(\mathbf{r}_i^{t+dt}, \tilde{\mathbf{v}}_i^{t+dt}) \\ \mathbf{v}_i^{t+dt} &= \mathbf{v}_i^t + \frac{1}{2} dt (\mathbf{f}_i^t + \mathbf{f}_i^{t+dt}). \end{aligned} \quad (6)$$

3.2 Chain model and scaling laws

When considering polymeric systems and especially biological ones like DNA strands, we find that both micro and macro dimensions are involved in the evolution of these systems. For instance the contour length of λ -phage DNA is $L = 21$ μm while its diameter is only few nanometers (~ 2 nm), and there are thus different length and time scales involved. This complexity requires a coarse-graining approach which ignores details of the polymer’s conformation under a certain length (for example the Kuhn length), to efficiently simulate the conformational changes. There are two methods for modeling chains at the coarse level: one is the bead-rod chain which models each segment of polymer with rigid links of fixed length (Kuhn

Table 1 Simulation parameter sets for WLC model

λ_p^{eff}	L_{sp}	$a_{\text{ff}} = a_{\text{pp}} = a_{\text{pf}}$	a_{wf}	a_{pw}
0.106	2	3.75	5.6	7.5

length); and the other is the bead-spring chain. In this work, we adopt the bead-spring representation of chain model which is a coarser model for polymer chains and has more flexibility than the bead-rod model. In addition to the standard conservative, dissipative, and random DPD interactions for every particle in the flow field, the polymer chains are subjected to intra-polymer forces (for each bead pair). The literature (Symeonidis et al. 2005) suggests several types of inter-bead potential forces such as Lennard-Jones, Hookean, Fraenkel stiff spring, finitely extensible nonlinear elastic (FENE) chain, and the worm-like chain (WLC). Since DNA (a rather stiff polymer) is the focus here, we select the WLC model with the pairwise interaction force given as

$$F_{ij}^{\text{WLC}} = -\frac{k_B T}{4\lambda_p^{\text{eff}}} \left[\left(1 - \frac{r_{ij}}{L_{\text{sp}}}\right)^{-2} + \frac{4r_{ij}}{L_{\text{sp}}} - 1 \right] \mathbf{e}_{ij} \quad (7)$$

where λ_p^{eff} is the effective persistence length which is the measure of the chain stiffness and L_{sp} is the maximum length of each chain segment. In the simulation of the DNA motion through the trap, the choice of persistence length is adopted from (Symeonidis et al. 2005) while the other chain parameters are shown in Table 1, where a_{ff} is the repulsive force coefficient between fluid–fluid particles, a_{pp} that between polymer–polymer, a_{pf} that between polymer–fluid, a_{wf} that between wall–fluid and a_{pw} that between polymer–wall. The choices of these coefficients are based on the results obtained in detailed exploration

of scaling laws, the quality of the solvent and the excluded volume effects. In addition to all the inter-particle forces, the electrical force (see next section) is applied on each bead according to the chain position in the channel.

Close examination of the scaling exponents of the chains’ radius of gyration R_g or end-to-end distance R with respect to the number of segments is required to determine the excluded volume effects and the solvent quality. The scaling theory for polymer solutions states that all physical properties and especially the polymer size can be expressed by the simple power law R or $R_g \approx (N)^\nu$. The static exponent is $\nu = 0.5$ for ideal chains, while in the case of good solvent, Flory (de Gennes 1979) found the exponent value using statistical scaling arguments, and obtained $\nu = 3/(d + 2)$, where d is the spatial dimension. Using more sophisticated techniques (Le Guillou and Zinn-Justin 1980) one can obtain the slightly more refined value of $\nu = 0.588$ compared to $\nu = 0.6$ in Flory’s formula.

In order to study the dynamics of polymers in a dilute solution, we perform simulations by immersing single chains of $N = 5, 10, 20, 50,$ and 100 beads in a periodic box (size 15 in each direction) of DPD particles. The chains’ mean radius of gyration and end-to-end distance is computed after it reaches the equilibrium condition and the results are shown in Fig. 2. It was investigated and concluded that the minimum ensemble of 50 chains is sufficient to obtain accurate data as a greater ensemble size yields the same results. We obtained the scaling exponent value of $\nu = 0.5521$ for radius of gyration and $\nu = 0.5759$ for end-to-end distance which is in a very good agreement to the value $\nu = 0.5516$ in Symeonidis et al. (2005) and eventually represents a fine consistency towards satisfying the excluded volume effects.

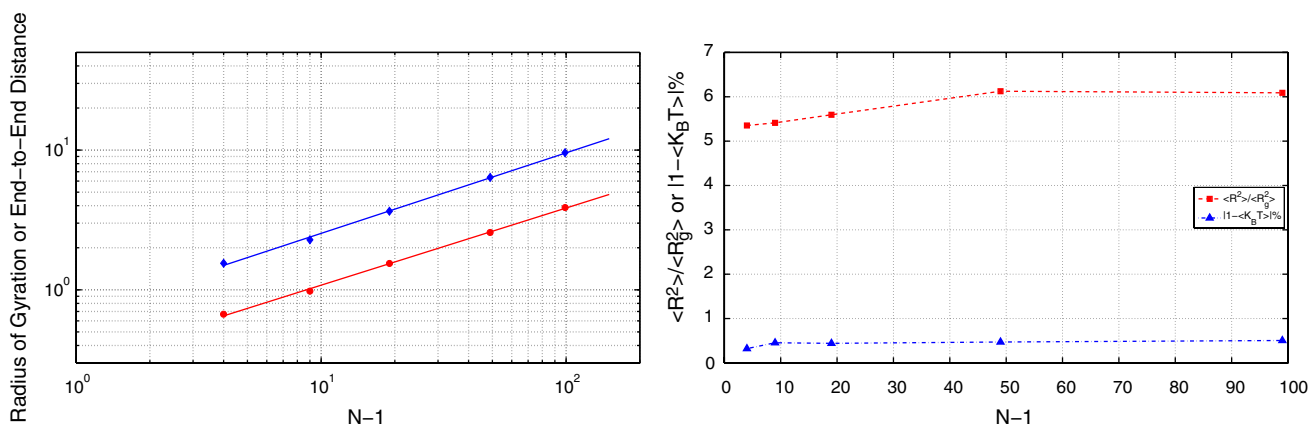


Fig. 2 Left scaling of radius of gyration (lower plot) and end-to-end distance (upper plot). Right the ratio $\langle R^2 \rangle / \langle R_g^2 \rangle$ (upper plot) and the chain temperature absolute error (lower plot). Simulation parameters: $L_{\text{sp}} = 2, \lambda_p^{\text{eff}} = 0.143, a_{\text{pf}} = a_{\text{ff}}, k_B T = 0.2$

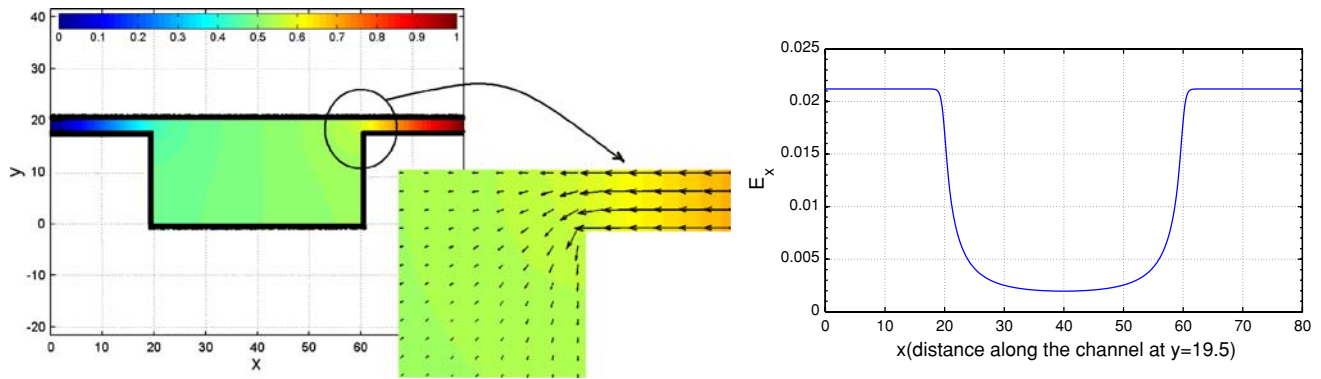


Fig. 3 *Left* the electric potential ϕ contour plot and representation of several electric field vectors near the slit. *Right* the x -component of the electric field inside the channel E_x , as a function of length of channel, measured along the plane in the middle of the shallow region

Table 2 The dimensions of the microchannel

L_d	L_s	t_d	t_s
40	40	20	2

3.3 Microchannel geometry and wall boundary conditions

The electrophoretic motion of DNA is mimicked by distributing uniform charges q among each of the beads in the chain. In order to find the driving force, the 2D electric potential $\phi(x, y)$ in the channel was determined by solving the Laplace equation $\nabla^2\phi = 0$. The equation was solved numerically, using a second-order finite difference scheme on a very refined mesh of size $\Delta x = \Delta y = 0.04$. The channel walls are insulated implying zero electric flux or von Neumann boundary conditions at surface boundaries ($\mathbf{n} \cdot \nabla\phi = 0$, where \mathbf{n} is the wall normal vector). We enforced the periodic voltage drop condition at the two sides of the slits $\phi(L, y) - \phi(0, y) = E_{av}L$, where L is the length of each period and E_{av} is the average electric field applied to the microchannel. Subsequently the nonuniform local electric field is obtained from the gradient of the electric potential $\mathbf{E} = -\nabla\phi$ and the electric force exerted on each bead is thus $\mathbf{F}_i^e = q\mathbf{E}$. In solving the Laplace equation for this case, it is sufficient to solve the equation for unit voltage drop ($\Delta V = E_{av}L = 1$). To obtain solutions for different potential differences, we only need to multiply the unity solution to the required voltage drop. We calculated the electric field unit by adjusting the mobility of the free-draining chain in a large unstructured microchannel, which is chain length independent and given by $\mu_0 = 1.84 \times 10^{-4} \text{ cm}^2/\text{V s}$ (Streek et al. 2005). Assuming a more refined approximation of $\mu_0 = 4.10 \times 10^{-4} \text{ cm}^2/\text{V s}$ (Nkodo et al. 2001) leads to $[E] \approx 220 \text{ V/cm}$. Hence the electric field

strength in a range of 10–110 V/cm corresponds to varying E_{av} in the range 0.0625–0.5. Figure 3 depicts the field contour plots of ϕ and x -component of the electric field for channel dimensions as indicated in Table 2. The plotted x -component of the electric field along the channel shows good agreement with the following approximation:

$$E_s = \frac{2t_d}{t_d + t_s} E_{av} = \frac{t_d}{t_s} E_d \tag{8}$$

where t_d and t_s are the depths of thick and shallow regions and E_d is the electric field strength at the well (see Fig. 1).

In DPD simulations we impose periodic boundary conditions on both the fluid and chain particles in the x (along two sides of the constriction) and z directions. Chain–wall interactions can be incorporated through adjustment of ρ_w , a_{pw} , and the type of boundary condition. The walls are simulated using the proposed random distribution of fixed particles and in order to prevent the chain and fluid particles penetrating to walls, we chose the density of wall particles $\rho_w = 6$ and applied the developed bounce normal reflection developed by the present authors and described in Moeendarbary et al. (2008).

In the proper application of periodic conditions for the chain beads and how these beads interact with each other and other solvent particles, it is advantageous to store the position of the chain beads in two different coordinates. The first is the unmapped or real chain coordinate which allows us to calculate the interbead forces. The second is the coordinate similar to the coordinate of all other particles which the polymer beads can freely move in and can have the periodic conditions similar to the solvent particles. The latter is helpful for estimating the interactions of polymer beads with solvent particles and we shall term these beads as ghost particles. It should be noted that both mentioned coordinates are identical when the chain

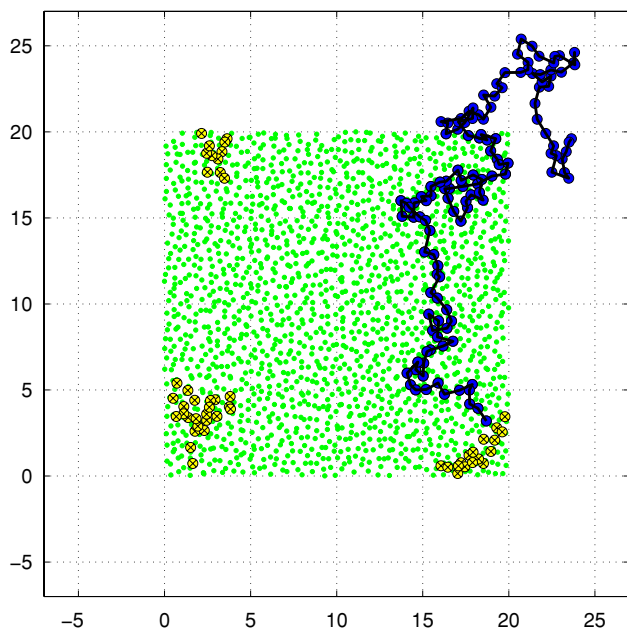


Fig. 4 The 2D representation of a 128 bead chain in a 20×20 simulation box. The *crossed circles* show the positions of the ghost chain beads, while the *small dots* represent the solvent particles

beads are in dimensions less than the box sizes. In Fig. 4 the schematic representation of both real and ghost chain particles is shown.

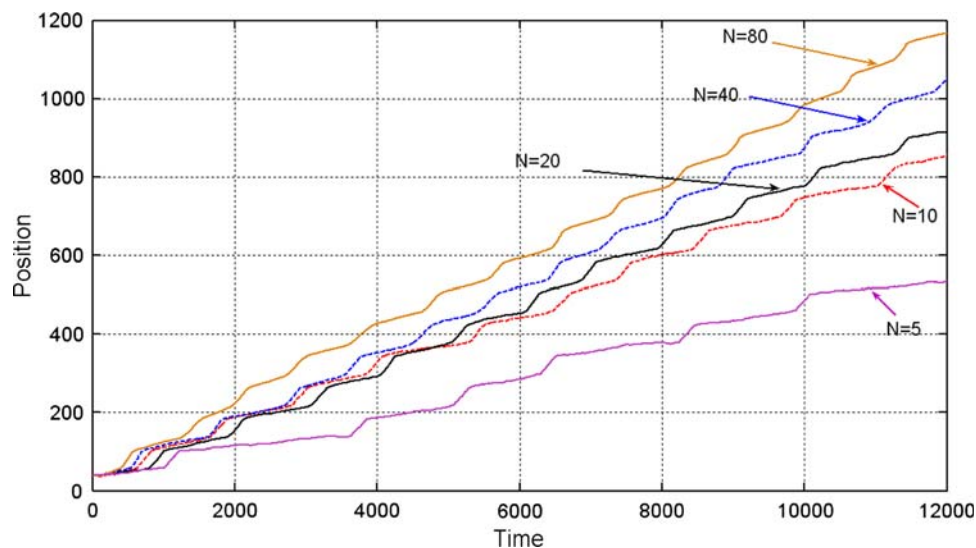
4 Results and discussions

In this section, the migration of DNA chains in microchannels is examined as we present the results of the present simulations. First the electric field was set to $E_{av} = 0.5$ and we calculate the x -component of the center

of mass trajectories for DNA chains of length $N = 5, 10, 20, 40$ and 80 , as shown in Fig. 5. This allows us to define the dimensionless mobility μ . We estimated μ as the slope of the line fitted through the x -component trajectory of the chain which has passed at least 20 periods. From Fig. 5, we observe that when the chain length increased, in addition to higher slope of the trajectories, they also became smoother. More specifically, for the longest chain of length $N = 80$, the steps in the trajectory appear smaller and gentler than the shortest chain of length $N = 5$.

In order to study the effects of the electric field strength and the chain length on mobility, we conducted several simulation runs. We performed runs for different chain lengths of $N = 10, 20, 40, 80, 160$, and 320 in average field values of $E_{av} = 0.0625, 0.125, 0.25$, and 0.5 . In order to obtain accurate results and to have ensemble of 50 chains, we run each case 10 times (ensemble of 10 chains) and allow the chain at each run to pass through at least 5 periods. Each run would require integration time of 3,000 (for long chains at high E_{av}) to 50,000 (for very short chains at low E_{av}) which takes 14–240 CPU hours on a single-core Intel[®] 2.66 GHz processor. To obtain better performance from the developed serial code, we used the Linux cluster of 32 dual-processor nodes to run our simulations. The estimated mobility μ as a function of N and E_{av} are plotted in Fig. 6. For all field values, we find that the longer chains travel faster. In this figure we observe that the mobility of the chain increased significantly when the chain length increased from $N = 40$ to $N = 80$ or 160 , and this is in a good qualitative agreement to the experimental observations of Han et al. (1999), Han and Craighead (2000, 2002). Furthermore, as the electric field is intensified, the mobility variation also becomes larger.

Fig. 5 The x -component of the center of mass trajectories of DNA chains of $N = 5, 10, 20, 40$ and 80 beads for the case of $E_{av} = 0.5$ and $L_{sp} = 4$



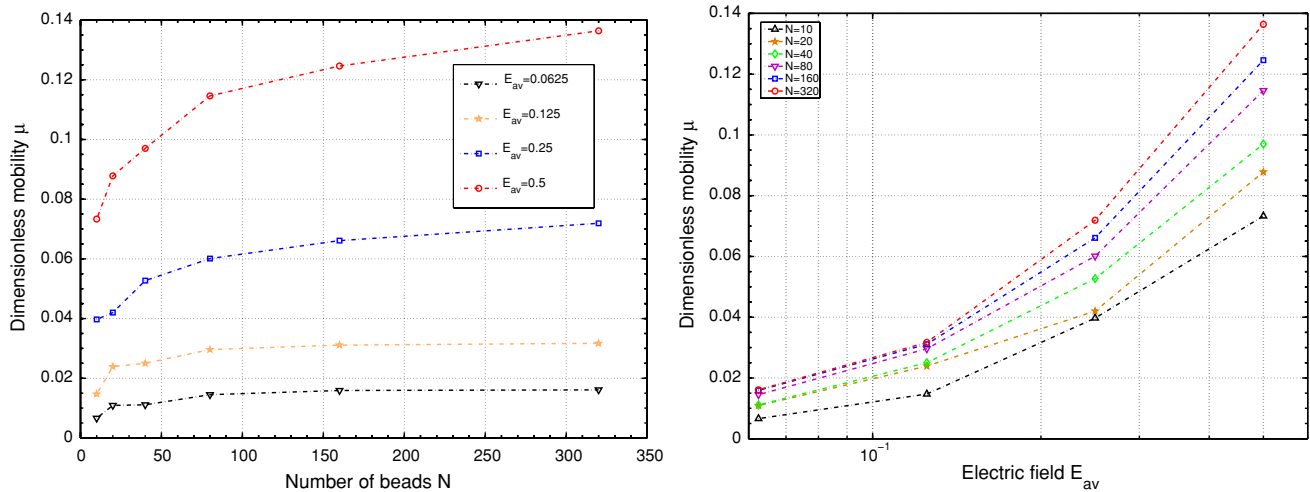


Fig. 6 *Left* dimensionless mobility μ of DNA chains for $E_{av} = 0.0625, 0.125, 0.25, 0.5$ as a function of N . *Right* dimensionless mobility μ of DNA chains for $N = 10, 20, 40, 80, 160, 320$ as a function of E_{av}

In this work, our main interest is the overall motion of the chains and our results generally show that the longer the chains, the greater the mobility. In addition and comparing to other previous numerical works the data in Fig. 6 (especially for the small chains in moderate fields) show overall better comparable agreement to the entropic trapping region of Fig. 3 in reference (Fu et al. 2006). Three regions are identified where chains of different sizes translate with different conformation and speed. Next we describe the mechanisms of chain migration in each region.

The first region is the well where the electric field lines are expanded and weakened so that the chain spends most of its migration time in this area. In this region the electric field lines are nonuniform and due to higher Brownian mobility, smaller chains are more probable to diffuse out of the field lines. This causes small molecules to reach the deeper areas or the corner of the well and be trapped there for longer times. The x – y trajectories of chains with $N = 5, 20$ and 80 are illustrated in Fig. 7. The effect of random Brownian diffusion from the field lines is more visible in high electric fields and for smaller molecules. Here the random motion depends on two dominant features, namely the length of the chain and the conformation of the molecule. When the chain is longer, it has more segments which come under influence of the electric field lines and so there is a very low probability of a sudden crossing of the molecule from its original smoothed pathway. In addition the relaxation time of a small chain is very low and as a result, when the molecule gets pushed out of the slit, it will quickly recoil. The coiled chains have little surface contact with the solvent

molecules and electric field lines so they would have higher random motion while long chains remain stretched and move in a smoother manner (see Figs. 5, 7).

The opening of the slit is the second region where several migration mechanisms are observed. From our results, we observe two main conformations by which the chains approach and pass through the opening of the gap; the hairpin and two ends escape. The formation of each state near the slit depends mainly on the size of the chain and the conformation of the chain as it approaches the gap from the well. Sebastian and Paul (2000) argued that the free-energy barrier for the “hairpin-escape” is twice that of the “two-ends-escape” because each hairpin can be considered as two chains crossing from the ends. Similar to Han et al. (1999), Han and Craighead (2000, 2002), they found that in the case of hernia formation and chain migration in the hairpin shape, the speed of escape is decreased as the chain length increased. However, when the chain approaches the slit through its end, they claimed that the speed of process is not dependent on molecule size since all linear chains have two ends. In our present simulations, we observed both mechanisms. However, when the chain becomes longer, we find that hairpin formation is the dominant mode of escape (see Figs. 8, 9 for two ends and hairpin migration of DNA chains). We note that for very small chains ($R_g \ll t_s$), none of the above mechanisms were present and the chain passes through the slit rapidly and without significant deformation.

Finally, we observe the speed of migration of molecules crossing through the shallow region (the third region in this discussion) is size-dependent and we expect it to increase with N as discussed in (Sebastian and Paul 2000). We

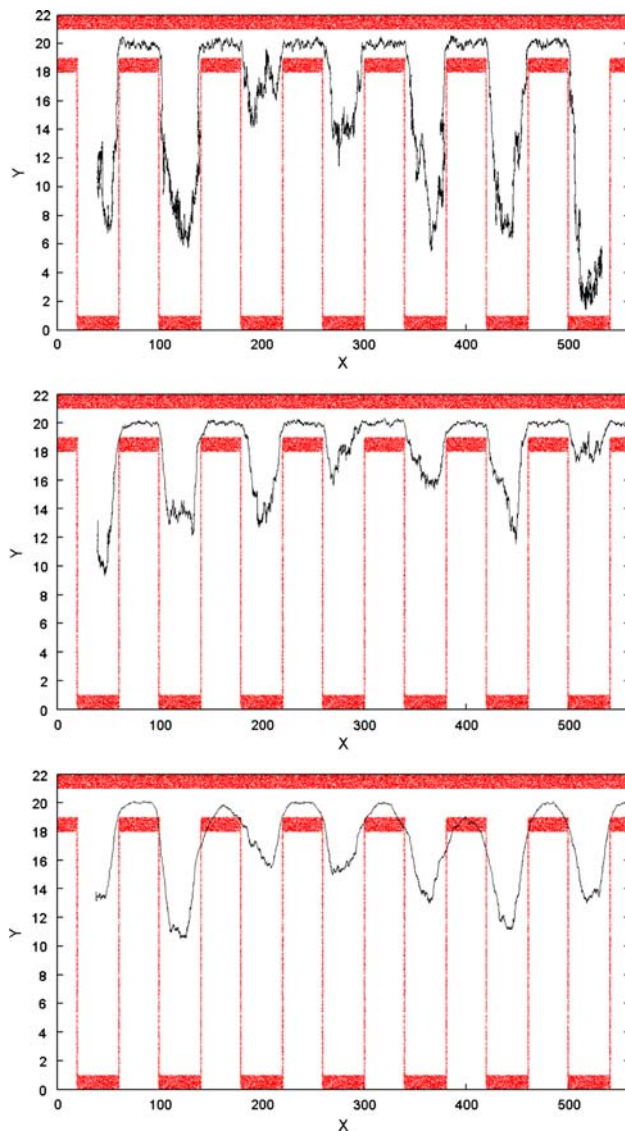


Fig. 7 Traverse (or xy) view of the center of mass trajectories of migrating DNA chains of different sizes through array for the case of $E_{av} = 0.5$ and $L_{sp} = 4$. *Top* $N = 5$. *Middle* $N = 20$. *Bottom* $N = 80$

observed that due to high-electric field strength, the DNA strands generally travel very fast in this region. Also, we note that when the DNA enters the slit from one of its ends, it would have the chance to stretch out and uncoil completely. In Fig. 8, the conformation evolution snapshots of a DNA chain with $N = 80$ approaching and passing the gap are shown. In this figure, the DNA is approaching with one end having a small hairpin formed. The DNA is completely uncoiled as it travels through the slit but recoils soon after exiting from the gap. In Fig. 9, the DNA approaches the slit while forming two hairpins in the middle of the chain. As the chain length increases, the probability of the number of hairpins which would be formed also increases, and this

assists in faster travel of the DNA from the entrance of the slit. The extension of the chain in z direction in order to form higher contact surface with the gap is the other physical trend which was generally observed for longer chains.

The DPD model which was used here can be further developed to fully incorporate some of the other deficiencies mentioned in Sect. 2 so that comparable quantitative results with experiment can be obtained for the optimization of device performance. In particular, the EOF from the walls can be imposed by introducing a small velocity slip (proportional to the zeta potential and the electric field strength) at the boundaries. Furthermore some amount of positive charges can be applied on the solvent particles which are positioned in specific distances (like Debye length) close to the chain beads to include the EOF and local flow around the DNA molecule.

5 Concluding remarks

We have carried out DPD simulations of DNA chains migrating through entropic traps, and our results generally show a good qualitative agreement with existing experimental data. The mesoscopic features of the DPD technique enabled us to capture the hydrodynamic interactions automatically. Three distinct regions where the chains migrate with different mechanisms were distinguished. Each region has different effects on the speed of the total process. Moreover, we observed several conformational phenomena which depend on chain length, the geometry of the microchannel, and the strength of the electric field. The chains formed hernias and were sucked into the gap while approaching the shallow region. The geometrical and field (electrical) conditions in the gap force the DNA chains to uncoil and travel smoothly through the slit. The chain then escapes from the gap and recoils in the deep region. According to the speed and form of relaxation and evolution of the chain in the well, it becomes ready to approach the next constriction. Two mechanisms are identified that cause the size-dependent trapping of DNA chains and thus mobility differences. First, small molecules are found to be trapped in the deep region due to higher Brownian mobility and crossing of electric field lines. Second, longer chains have higher probability to form hernias at the entrance of the gap subsequently enabling them to pass the entropic barrier more easily. Consequently, longer DNA molecules have higher mobility and travel faster than shorter chains.

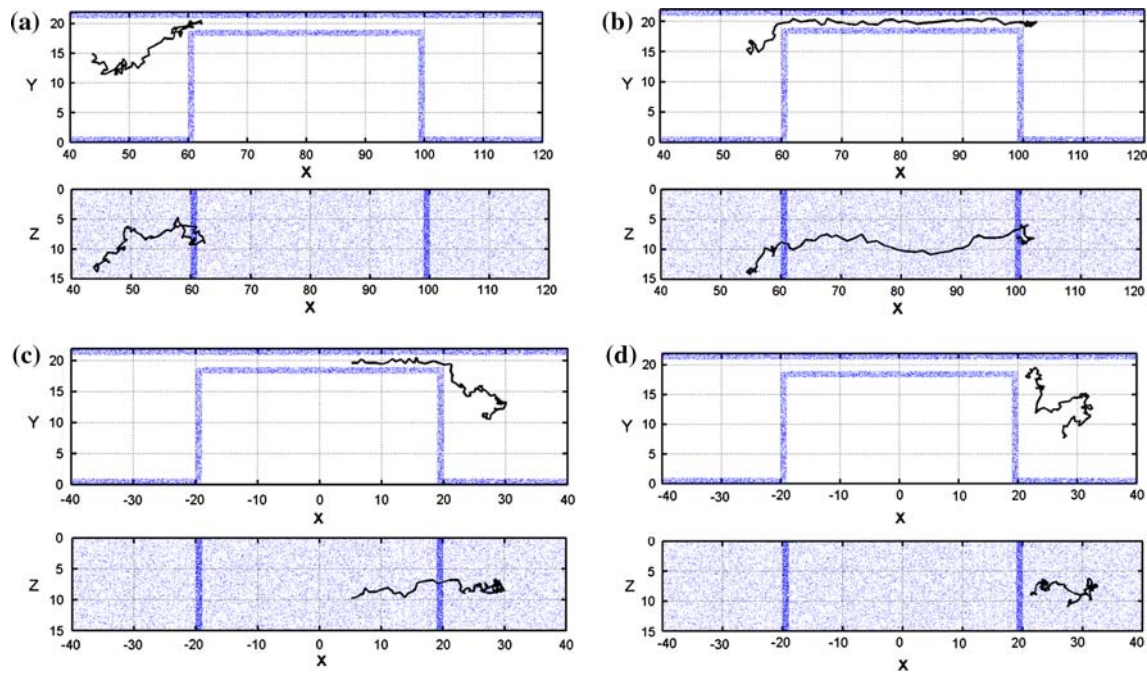


Fig. 8 Conformation evolution snapshots of DNA chain with $N = 80$ beads passing through trap for case of $E_{av} = 0.5$ and $L_{sp} = 4$. Traverse (or xy) and top (or xz) views of translations from (a) time $t = 3,600$ to (c) time $t = 4,000$

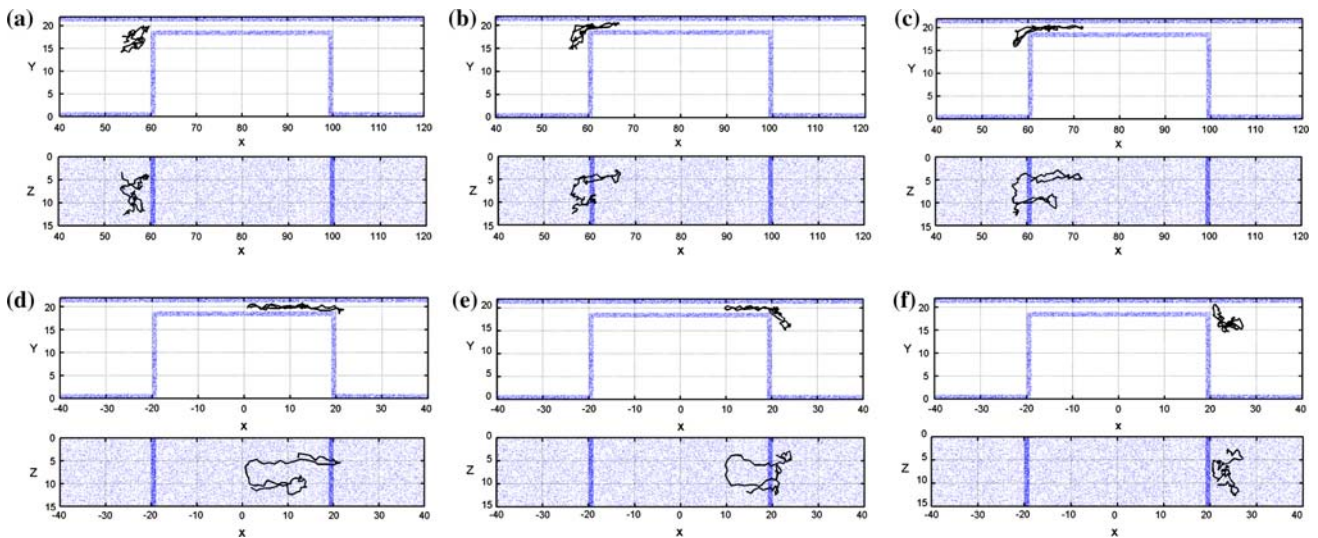


Fig. 9 Conformation evolution snapshots of DNA chain with $N = 80$ beads passing through trap for case of $E_{av} = 0.5$ and $L_{sp} = 4$. Traverse (or xy) and top (or xz) views of translations from (a) time $t = 5,520$ to (f) time $t = 5,820$

Acknowledgment The first author, E. Moeendarbary, is grateful for the support of the Singapore Agency for Science, Technology and Research (A*STAR) through the International Graduate Scholarship.

References

André P et al (1998) Polyelectrolyte/post collisions during electrophoresis: influence of hydrodynamic interactions. *Eur Phys J B Condens Matter* 4(3):307–312

Chen Z, Escobedo FA (2003) Simulation of chain-length partitioning in a microfabricated channel via entropic trapping. *Mol Simul* 29(6):417–425
 Cheng KL et al (2008) Electrophoretic size separation of particles in a periodically constricted microchannel. *J Chem Phys* 128:101101
 de Gennes PG (1979) *Scaling concepts in polymer physics*. Cornell University Press, Ithaca
 Espanol P, Warren P (1995) Statistical-mechanics of dissipative particle dynamics. *Europhys Lett* 30(4):191–196
 Fan X et al (2006) Simulating flow of DNA suspension using dissipative particle dynamics. *Phys Fluids* 18(6):063102-10

- Fan X et al (2003) Microchannel flow of a macromolecular suspension. *Phys Fluids* 15(1):11–21
- Fedosov DA, Em Karniadakis G, Caswell B (2008) Dissipative particle dynamics simulation of depletion layer and polymer migration in micro- and nanochannels for dilute polymer solutions. *J Chem Phys* 128(14):144903–144914
- Fu J, Yoo J, Han J (2006) Molecular sieving in periodic free-energy landscapes created by patterned nanofilter arrays. *Phys Rev Lett* 97(1):18103
- Groot RD, Rabone KL (2001) Mesoscopic simulation of cell membrane damage, morphology change and rupture by nonionic surfactants. *Biophys J* 81(2):725–736
- Groot RD, Warren PB (1997) Dissipative particle dynamics: bridging the gap between atomistic and mesoscopic simulation. *J Chem Phys* 107(11):4423–4435
- Han J, Craighead HG (2000) Separation of long DNA molecules in a microfabricated entropic trap array. *Science* 288(5468):1026–1029
- Han J, Craighead HG (2002) Characterization and optimization of an entropic trap for DNA separation. *Anal Chem* 74(2):394–401
- Han J, Turner SW, Craighead HG (1999) Entropic trapping and escape of long DNA molecules at submicron size constriction. *Phys Rev Lett* 83(8):1688–1691
- He YD et al (2007) Polymer translocation through a nanopore in mesoscopic simulations. *Polymer* 48(12):3601–3606
- Hoogerbrugge PJ, Koelman J (1992) Simulating microscopic hydrodynamic phenomena with dissipative particle dynamics. *Europhys Lett* 19(3):155–160
- Jendrejack RM, de Pablo JJ, Graham MD (2002) Stochastic simulations of DNA in flow: dynamics and the effects of hydrodynamic interactions. *J Chem Phys* 116:7752
- Jiang W et al (2007) Hydrodynamic interaction in polymer solutions simulated with dissipative particle dynamics. *J Chem Phys* 126(4):044901–044912
- Kubo R (1966) The fluctuation–dissipation theorem. *Rep Prog Phys* 29:255–284
- Le Guillou JC, Zinn-Justin J (1980) Critical exponents from field theory. *Phys Rev B* 21(9):3976–3998
- Lee YM, Joo YL (2007) Brownian dynamics simulations of polyelectrolyte molecules traveling through an entropic trap array during electrophoresis. *J Chem Phys* 127:124902
- Li Z, Drazer G (2008) Hydrodynamic interactions in dissipative particle dynamics. *Phys Fluids* 20(10):103601–103608
- Long D, Viovy JL, Ajdari A (1996) Simultaneous action of electric fields and nonelectric forces on a polyelectrolyte: motion and deformation. *Phys Rev Lett* 76(20):3858–3861
- Marsh CA, Backx G, Ernst MH (1997) Static and dynamic properties of dissipative particle dynamics. *Phys Rev E Stat Phys Plasmas Fluids Relat Interdiscip Top* 56(2):1676–1691
- Millan JA et al (2007) Pressure driven flow of polymer solutions in nanoscale slit pores. *J Chem Phys* 126(12):124905–124909
- Moeendarbary E, Lam KY, Ng TY (2008) A new “bounce-normal” boundary in DPD calculations for the reduction of density fluctuations. In: 2008 Proceedings of the ASME Micro/Nanoscale Heat Transfer International Conference, MNHT 2008
- Nkodo AE et al (2001) Diffusion coefficient of DNA molecules during free solution electrophoresis. *Electrophoresis* 22(12):2424–2432
- Pan W et al (2008) Hydrodynamic interactions for single dissipative-particle-dynamics particles and their clusters and filaments. *Phys Rev E Stat Nonlinear Soft Matter Phys* 78(4):046706–046712
- Panwar AS, Kumar S (2006) Time scales in polymer electrophoresis through narrow constrictions: a Brownian dynamics study. *Macromolecules* 39(3):1279–1289
- Sebastian KL, Paul AKR (2000) Kramers problem for a polymer in a double well. *Phys Rev E* 62(1):927–939
- Streek M et al (2004) Mechanisms of DNA separation in entropic trap arrays: a Brownian dynamics simulation. *J Biotechnol* 112(1–2):79–89
- Streek M et al (2005) Two-state migration of DNA in a structured microchannel. *Phys Rev E Stat Nonlinear Soft Matter Phys* 71(1):11905
- Symeonidis V, Em Karniadakis G, Caswell B (2005) Dissipative particle dynamics simulations of polymer chains: scaling laws and shearing response compared to DNA experiments. *Phys Rev Lett* 95(7):76001
- Tessier F, Labrie J, Slater GW (2002) Electrophoretic separation of long polyelectrolytes in submolecular-size constrictions: a Monte Carlo study. *Macromolecules* 35(12):4791–4800
- Viovy JL (2000) Electrophoresis of DNA and other polyelectrolytes: physical mechanisms. *Rev Mod Phys* 72(3):813–872